Protein Coating of DNA Nanostructures for Enhanced Stability and Immunocompatibility

Auvinen, Henni

2017-09-20

Auvinen , H , Zhang , H , Nonappa , Kopilow , A , Niemelä , E H , Nummelin , S , Correia , A , Santos , H A , Linko , V & Kostiainen , M A 2017 , ' Protein Coating of DNA Nanostructures for Enhanced Stability and Immunocompatibility ' , Advanced Healthcare Materials , vol. 6 , no. 18 , 1700692 . https://doi.org/10.1002/adhm.201700692

http://hdl.handle.net/10138/248402
https://doi.org/10.1002/adhm.201700692

unspecified
publishedVersion

ADVANCED HEALTHCARE MATERIALS

www.advhealthmat.de

Protein Coating of DNA Nanostructures for Enhanced Stability and Immunocompatibility

Henni Auvinen, Hongbo Zhang, Nonappa, Alisa Kopilow, Elina H. Niemelä, Sami Nummelin, Alexandra Correia, Hélder A. Santos, Veikko Linko, and Mauri A. Kostiainen**

Fully addressable DNA nanostructures, especially DNA origami, possess huge potential to serve as inherently biocompatible and versatile molecular platforms. However, their use as delivery vehicles in therapeutics is compromised by their low stability and poor transfection rates. This study shows that DNA origami can be coated by precisely defined one-to-one protein-dendron conjugates to tackle the aforementioned issues. The dendron part of the conjugate serves as a cationic binding domain that attaches to the negatively charged DNA origami surface via electrostatic interactions. The protein is attached to dendron through cysteine-maleimide bond, making the modular approach highly versatile. This work demonstrates the coating using two different proteins: bovine serum albumin (BSA) and class II hydrophobin (HFBI). The results reveal that BSA-coating significantly improves the origami stability against endonucleases (DNase I) and enhances the transfection into human embryonic kidney (HEK293) cells. Importantly, it is observed that BSA-coating attenuates the activation of immune response in mouse primary splenocytes. Serum albumin is the most abundant protein in the blood with a long circulation half-life and has already found clinically approved applications in drug delivery. It is therefore envisioned that the proposed system can open up further opportunities to tune the properties of DNA nanostructures in biological environment, and enable their use in various delivery applications.

DNA nanotechnology has taken a giant leap toward real-life applications during the recent years.[1,2] After the invention of DNA origami in 2006,[3] the whole research field has grown exponentially.[2,4] Today there are numerous ways to build discrete user-defined, accurate, and fully addressable DNA nanostructures, such as scaffolded 2D and 3D origami[3,5,6] with twists, curves, and bends,[7,8] Lego-like objects formed from molecular canvases,[9] and wireframe-based meshed constructions.[10–12] The computational tools[11–13] for designing such objects have emerged along with these techniques, and this progress has opened up new possibilities for the researchers to effortlessly build their own nanostructures for tailored uses.[14] Recently demonstrated applications based on customized DNA nanostructures include artificial ion channels,[15] optical (plasmonic and photonic) structures,[16,17] high-precision molecular positioning devices,[18] modifiable templates for arranging, e.g., proteins,[19–21] polymers,[22] and nanotubes,[23] as well as DNA-assisted techniques for creating arbitrarily shaped metal nanoparticles.[24–26]

H. Auvinen, A. Kopilow, Dr. S. Nummelin, Dr. V. Linko, Prof. M. A. Kostiainen
Department of Bioproducts and Biosystems
Aalto University
FI-00076 Aalto, Finland
E-mail: veikko.linko@aalto.fi; mauri.kostiainen@aalto.fi

Prof. H. Zhang, A. Correia, Prof. H. A. Santos
Drug Research Program, Division of Pharmaceutical Chemistry and Technology
Faculty of Pharmacy
University of Helsinki
FI-00014 Helsinki, Finland

Prof. H. Zhang
Department of Pharmaceutical Sciences
Åbo Akademi University
FI-20520 Turku, Finland

Dr. Nonappa
Molecular Materials, Department of Applied Physics
Aalto University
FI-00076 Aalto, Finland

Dr. E. H. Niemelä
Research Programs Unit, Faculty of Medicine
University of Helsinki
P.O. Box 63, FI-00014 Helsinki, Finland

Prof. H. A. Santos
Helsinki Institute of Life Science
University of Helsinki
Helsinki FI-00014, Finland

The ORCID identification number(s) for the author(s) of this article can be found under https://doi.org/10.1002/adhm.201700692.

DOI: 10.1002/adhm.201700692

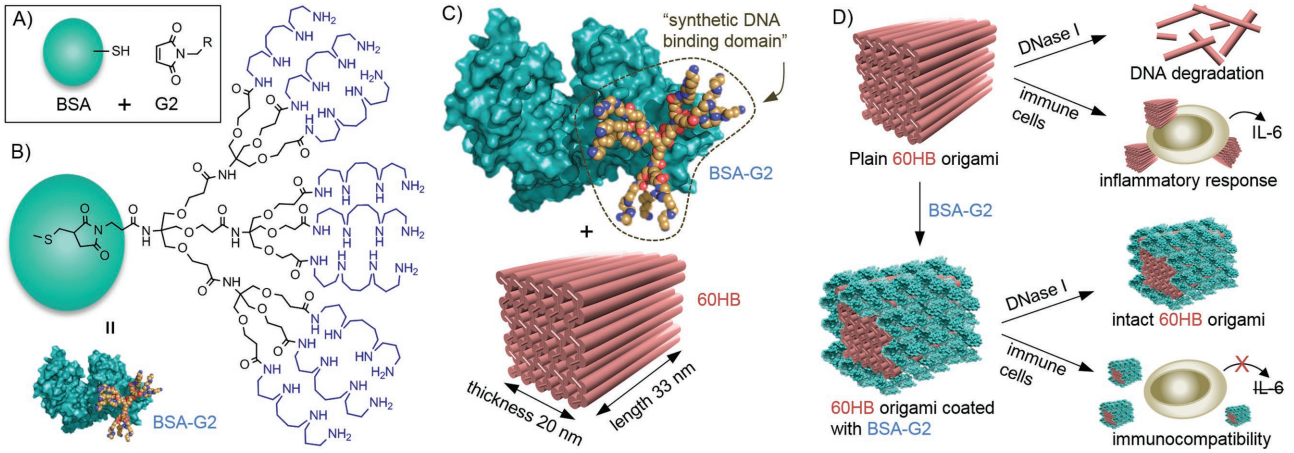

Figure 1. Schematics of the protein–dendron coating of DNA origami nanostructures. A) Bovine serum albumin (BSA) is anchored to the second-generation dendron (G2) via a cysteine–maleimide bond. B) The structure of the whole BSA-G2 conjugate. C) BSA-G2 can be attached to a brick-like DNA origami (60-helix bundle, 60HB) via electrostatic binding: a positively charged domain of BSA-G2 binds to a negatively charged surface of the DNA origami. D) BSA-G2 coating of DNA origami provides protection against endonucleases, attenuates immune activation, and enhances cellular delivery rates of the nanostructures.

In addition to these applications, an increasing effort has been put into applying DNA nanostructures as smart drug-delivery vehicles and biomolecular devices at the cellular level.[27–30] These examples cover logic-gated nanorobots for modulating cell signaling,[31] structures for delivering anti-cancer drugs[32–34] and for circumventing drug-resistance,[35,36] as well as carriers equipped with siRNA molecules,[37] CpG-triggers,[38] and functional enzymes.[39] Despite this progress, it has been observed that the transfection of DNA structures is generally low[40] and that these objects are prone to degradation in biological environment.[41] Nevertheless, there exist techniques to presumably enhance both stability and transfection rates of the DNA structures by utilizing different sophisticated protection and coating mechanisms, such as virus protein[42] or lipid membrane encapsulation.[43] It has also been shown that spermidine-stabilized structures could be efficiently transfected by electroporation.[44] Moreover, it has been suggested that the delivery rates could be improved by employing DNA intercalators,[45] by directly incorporating specific proteins into the structures,[46] or by using cationic polymer coating.[47–49] For DNA binding and coating purposes, dendrons and dendrimers are ideal polymer structures.[50,51] They are regularly branched synthetic molecules with essentially monodisperse structure[52] and high density of functional groups capable of binding various biomolecules with high affinity through multivalent and multimodal interactions.[53] Thus, they provide access to synthetic macromolecules with a primary structure of the same level of precision as DNA origami, proteins, or other biological molecules.[54]

Biohybrid structures that further combine synthetic polymers with biological macromolecules can bring together the best features of both material types—the versatility of synthetic materials and highly specific biological properties. Synthetic polymers attached on a protein surface can, for example, provide augmented or entirely new features to the unique biological property of the protein. Examples of such enhancements include improved pharmacokinetic properties,[55] stimuli-responsive properties (e.g., modulation of enzyme activity, selective purification by phase separation, and size-dependent binding),[56] formation of higher-order structures,[57] and biosensing and binding to new targets.[58]

Here, we present a straightforward and versatile method to protect DNA origami nanostructures by coating them with protein coronas. The method is solely based on electrostatic interactions between protein–dendron conjugates and a DNA origami (**Figure 1**), and, therefore, it provides an attractive alternative to the other protection techniques[43] and protein coatings[46] that are based on the modifications of the individual DNA strands in the complex structure or hydrophobic interactions.[59]

We demonstrate the feasibility of the conjugation by anchoring two different proteins to the dendron via a cysteine–maleimide bond: bovine serum albumin (BSA; Figure 1A, B) and class II hydrophobin (HFBI). As a reference we also used three facially different Janus dendrimers. All structures are shown in Figure S1 in the Supporting Information. The multivalent dendron part of the conjugate acts as a (cationic) synthetic DNA binding domain that attaches to negatively charged 60-helix bundle (60 HB, dimensions of 20 nm × 20 nm × 33 nm) DNA origami surface (Figure 1C). 60HB serves here as a model structure and has the dimensions of a regular hexagonal or square lattice 3D origami prepared with the M13 scaffold. By adjusting the concentration ratio of conjugates versus origami, it is possible to achieve a complete and dense protein shield for the origami structures (Figure 1D). In this work, we observed that especially BSA coating of the origami gives promising results, as the transfection rates can be enhanced 2.5-fold compared to bare origami. Remarkably, the coating also provides full protection against DNase I endonuclease, whereas under the same experimental conditions the plain origami gets completely degraded (Figure 1D). The binding efficiency was examined using gel electrophoretic mobility shift assay (EMSA) and transmission electron microscopy (TEM). As the potential use DNA origami nanostructures for therapeutic purposes require intravital administration, we wished to ascertain

the immunocompatibility of our nanostructures. Appropriately, the BSA-based coating of the structures was shown to attenuate immune activation of the mouse primary splenocytes (Interleukin 6 (IL-6) assay), similarly as recently demonstrated for albumin-coated virus particles (Figure 1D).[60] In addition, we tested if the combination of reference Janus dendrimers could form a bilayer coating over DNA origami (results are shown in the Supporting Information).

60-helix bundles were prepared as described previously[61] and the excess staple strands were removed by poly(ethylene glycol)-based purification[62] (see also the Supporting Information for details). The purified 60HBs (constant concentration of 4.4×10^{-9} M) were mixed with increasing concentrations of protein–dendron conjugates (synthesized as previously reported[63,64]) in an aqueous solution. Two different dendron generations were used: generation 1 (G1) contains nine protonatable amines (HFBI-G1 and BSA-G1) and the second generation (G2) includes 27 amines that can be protonated (HFBI-G2 and BSA-G2). The unique structural property of these protein–polymer conjugates is their precisely defined, one-to-one structure where the conjugation site (one free cysteine) is exactly known. Therefore, such conjugates minimize dispersity issues and can provide clear structure–property relationships.

The results were analyzed using gel EMSA, as shown in **Figure 2**A. The conjugate concentration/origami concentration ratio (c_C/c_O) was varied between 0–3000 for HFBI dendrons and 0–2000 for BSA dendrons. As can be seen in Figure 2, G1 dendrons did not show any binding within the studied concentration range. However, EMSA with G2 dendrons clearly reveals interactions between the conjugates and the origami. HFBI-G2 and 60HBs tend to aggregate at high concentrations (c_C/c_O = 1000–3000) as the leading band gets dimmer, but the band in front of the well becomes more intense (the leading band completely disappears at c_C/c_O = 3000). In the case of BSA-G2, the band is clearly shifting at c_C/c_O = 1000 and 2000, indicating a proper binding without undesired aggregation.

TEM analysis (Figure 2B–D) confirms the EMSA result: 60HBs and BSA-G2 conjugates form discrete objects, whereas HFBI-G2 forms large aggregates (see the Supporting Information). The larger size and inert nature of BSA helps to prevent dendron-mediated cross-linking (also avoiding hydrophobic interactions in the case of HFBI) and consequently yields origami structures coated with a single protein layer. It can be readily observed that the bare origami (Figure 2B) and the BSA-coated origami (Figure 2C) have distinct morphologies, and the quantitative analysis of the dimensions of the objects (Figure 2D) further proves the dense and relatively uniform protein coating. The measured dimensions of 60HB (thickness of 19.4 ± 1.8 nm and length of 33.4 ± 2.1 nm) precisely correspond to the designed dimensions (thickness of 20 nm and length of 33 nm), whereas dimensions of the BSA-G2-coated 60HB are extended on average by 12 nm compared to the plain 60HB (thickness of 31.1 ± 5.1 nm and length of 45.7 ± 6.5 nm). This observation implies that the origami structures are coated with a dense shield of proteins (BSA-G2 dimensions ≈7 nm × 6 nm × 6 nm).

After the protein–dendron coating was verified and optimized, the transfection properties of the complexes were examined in vitro. For that, the origami structures were labeled with AlexaFluor 488 dye (six dyes per origami) and transfected to human embryonic kidney cells (HEK293) with and without the protein coating (see the Supporting Information). Transfection was studied using two different origami concentrations (0.64×10^{-9} M and 1.28×10^{-9} M), and for coating, both HFBI-G2 and BSA-G2 were added at a ratio of c_C/c_O = 2000. The cells were incubated for 12 h with the samples, after which their viability was verified, and the fixed cells (nuclear staining with 4′,6-diamidino-2-phenylindole (DAPI)

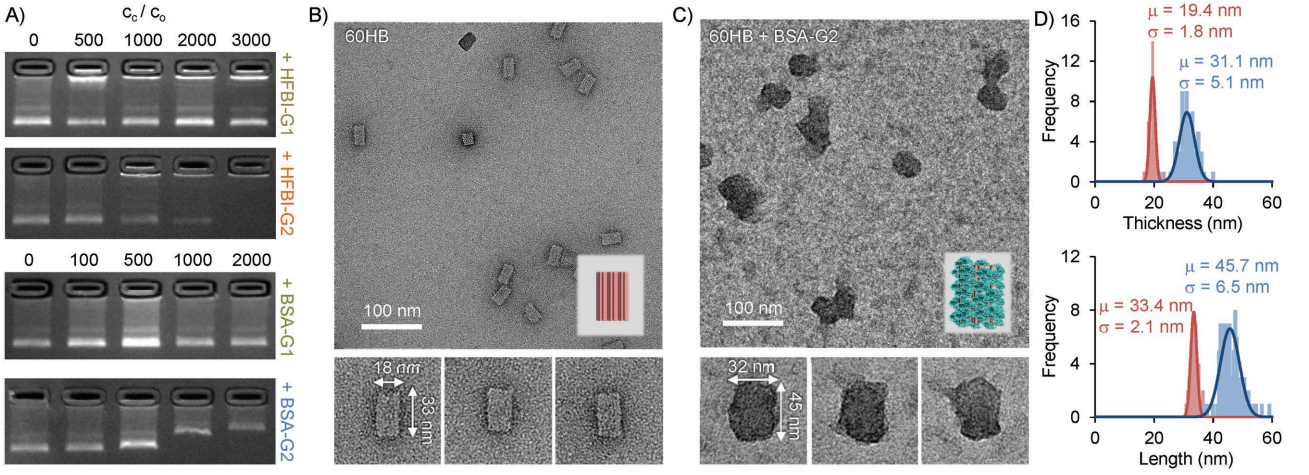

Figure 2. Gel EMSA and TEM micrographs of the samples. A) Agarose gel EMSA of a constant amount of DNA origami (c_O = origami concentration = 4.4×10^{-9} M) complexed with increasing amounts of HFBI-G1, HFBI-G2, BSA-G1, and BSA-G2 conjugates (c_C/c_O = conjugate concentration/origami concentration). EMSA indicates low binding efficiency of both G1 conjugates, whereas HFBI-G2 induces aggregation of the complexes. However, EMSA reveals successful complexation of BSA-G2 and DNA origami as the origami bands clearly shift at concentrations c_C/c_O = 1000 and 2000 (bottom panel). B,C) The BSA-G2 complexation is confirmed by TEM as the shape and the dimensions of the objects are changing. B) Plain 60HB (negative staining) and C) BSA-G2-coated 60HB (c_C/c_O = 2000). The size of the insets is 80 nm × 80 nm. D) Analysis of the object dimensions (thickness and length) determined from the TEM images. The dimensions (curves show Gaussian fits) of the plain 60HB are shown in red and BSA-G2-coated 60HB (c_C/c_O = 2000) in blue.

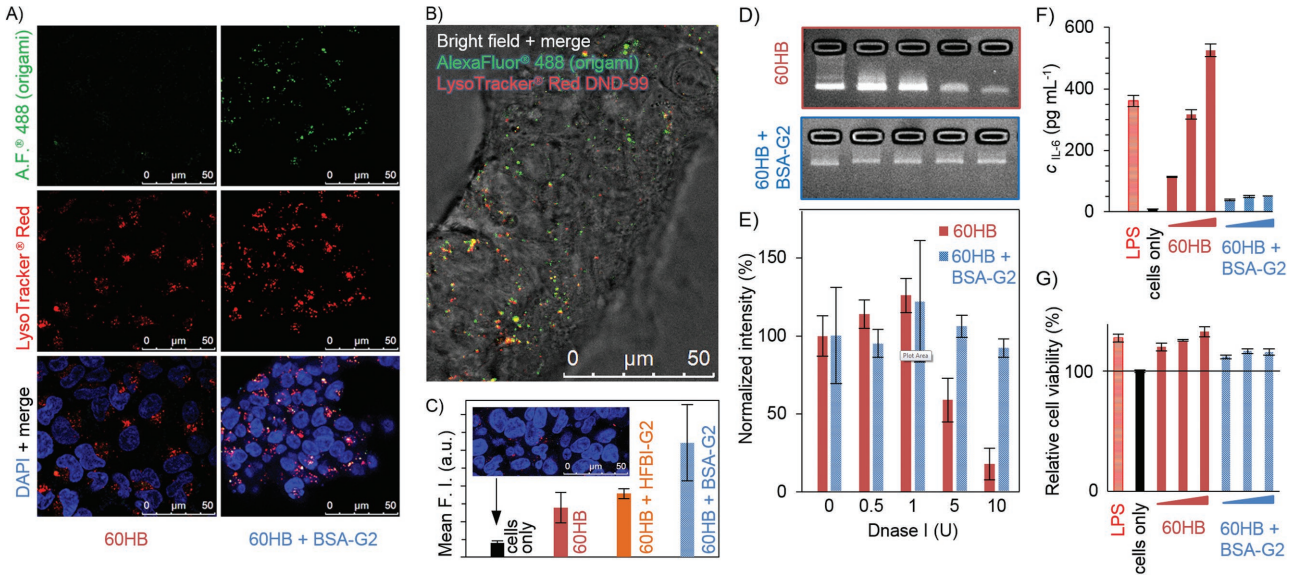

Figure 3. A) Confocal micrographs of HEK293 cells after 12 h transfection with DNA origami. Left: 60HB, and right: BSA-G2-coated origami. The top panel (AlexaFluor 488, green) is the origami channel, the middle panel (LysoTracker, red) shows the lysosomes, and the bottom panel contains DAPI-stained nuclei and an overlay image of the top and the middle panel. B) Transfection of the BSA-G2-coated origami structures with bright field image of the cells. C) Quantification of the transfection efficiency (mean fluorescence intensity (F. I.)) by flow cytometry. The inset depicts cells only control sample. The data consist of the average values measured from two independent sample sets (data are expressed as mean ± data range, $n \geq 3$). D) BSA-G2-based protection of DNA origami against endonuclease (DNase I). It shows the gel electrophoresis of 60HB (D, top) and 60HB coated by BSA-G2 (D, bottom) with increasing amount of added DNase I (identical for both gels). E) The normalized intensity of DNA origami bands calculated from three different gels (data are expressed as mean ± SD, $n = 3$). F) Production of IL-6 by mouse primary splenocytes. Cells were incubated with 60HB and 60HB+BSA-G2 (0.08, 0.28, and 0.88 × 10^{-9} M) for 20 h (data are expressed as mean ± data range, $n = 2$). G) Splenocyte viability. Cells were treated for 20 h as in panel (C), followed by viability assay for 24 h (data are expressed as mean ± data range, $n = 2$).

was carried out after fixing) were imaged using confocal fluorescence microscopy, as shown in **Figure 3** (1.28×10^{-9} M data shown here, and 0.64×10^{-9} M data and HFBI-G2 coating are in the Supporting Information). The confocal micrographs show that the transfection efficiency for bare origami and HFBI-G2-coated origami is low (see Supporting Information). However, with the BSA-G2 coating, the transfection is clearly improved (Figure 3A, right). In addition, it can be seen that in some cases BSA coating may enhance endosomal escape of the complexes as the lysosomes (LysoTracker, red) and the origami (AlexaFluor 488, green) are not co-localized (Figure 3B). However, uncoated and HFBI-coated 60HBs are not observed outside lysosomes in the same extent (see the Supporting Information). It is known that DNA nanostructures coated with proteins or other designer materials can be bound nonspecifically on cell surfaces and taken up via endocytosis. Here, the BSA-G2-coated 60HB most probably follows the same pathway, which is promoted by the nonaggregated state and the discrete object size of the complex.

To further verify these results, the transfection efficiency was quantified using flow cytometry. The origami concentration in these experiments was adjusted to 0.32×10^{-9} M ($c_C/c_O = 2000$), and the results can be seen in Figure 3C. In general, the mean fluorescence intensity (that depicts the transfection efficiency) increases as the origami is coated with proteins. However, HFBI coating enhances the transfection only slightly, but by employing BSA coating, the transfection rate can be improved by a factor of 2.5 compared to bare origami. The observed differences between BSA and HFBI can be related to the sample morphology, which in the case of HFBI coating is heavily aggregated, lowering the transfection efficiency.

As the combination of BSA-G2 and the origami promisingly yields discrete and densely coated complexes with enhanced transfection properties, it is of high importance to study their structural integrity for the foreseen delivery applications. The potential protection of the protein coating was examined by exposing plain origami ($c_O = 3.3 \times 10^{-9}$ M) and BSA-G2-coated structures ($c_O = 3.3 \times 10^{-9}$ M, $c_C/c_O = 2000$) to DNase I digestion (0–10 U in 20 µL sample volume) for 1 h at room temperature, after which their viability was verified by gel electrophoresis. The intensities are obtained by integrating over the gel band, and the average value for the "0 U" sample is normalized to 100 %. As can be seen from Figure 3D,E, the bare origami degrades almost completely as the nuclease concentration is increased. However, the BSA-coated structures retain their migration speed and band intensity throughout the concentration range, which further indicates that the BSA coating is dense and that the coating efficiently protects the DNA structure from nuclease degradation. As a comparison, the Janus dendrimer-based coating resulted in less than 50% viability at the maximum concentration 10 U/20 µL (see the Supporting Information for details).

In this work we have used IL-6 secretion from splenic immune cells as readout for immune stimulation, as IL-6 is a proinflammatory cytokine produced by antigen presenting cells (APCs) in the acute phase of inflammation. Naked DNA molecules are internalized by APCs and act as pathogen-associated molecular patterns, activating the immune system via TLR9,

which leads to the production of proinflammatory cytokines. TLR9 signals via the NF-κB pathway, driving the expression of IL-6.[65] To assess the immune reactivity of the origami before and after coating, mouse primary splenocytes were harvested and treated immediately with increasing concentrations (0.08, 0.28, and 0.88×10^{-9} M) of noncoated and coated 60HBs. Immune stimulation was assessed by measuring the production of IL-6, with bacterial lipopolysaccharide (LPS) as a positive control. We observed a robust immune reaction from both LPS and uncoated origami, which was significantly attenuated by coating with BSA-G2 (Figure 3F). As evidenced by the TEM images, the BSA layer covering the origami is dense enough to mask the DNA core from detection by immune receptors. At the highest origami concentration, we observed over ten-fold decrease in the IL-6 production. Importantly, cell viability was similar in all of the treatments, demonstrating that lack of immune activation is not due to cell death (Figure 3G). Taken together, we demonstrate excellent biocompatibility and escape from immune response as a result of DNA origami coating with BSA-G2.

As a conclusion, we have demonstrated an easily attainable method to improve the properties of DNA origami nanostructures for the delivery applications. We have shown that the stability and the transfection rates of DNA origami can be enhanced by coating them electrostatically with protein–dendron conjugates. Any protein that can be attached to the synthetic DNA-binding dendron via a cysteine–maleimide bond is suitable for the coating, but the electric charge of the protein should be taken into account in order to avoid undesired aggregation. Here, we observed that especially the BSA coating protects the DNA origami from the nuclease degradation and improves the transfection to HEK cells. Furthermore, we showed that it is possible to "shield" the DNA nanocarriers from immune surveillance by complete serum albumin coating. As our approach is highly versatile, and therefore feasible for other proteins, we believe that the presented technique is a substantial addition to the ever-extending family of DNA-based delivery approaches[28–30] that serve as compelling alternatives to polymer, nanoparticle, and virus-based delivery methods.

Experimental Section

Materials for dendrimers and dendrons, details on DNA origami fabrication and purification, formation of protein–dendron–origami complexes, gel electrophoresis, DNase I assay, TEM and cryo-EM imaging, transfection and confocal imaging, flow cytometry, splenocyte IL-6 activation assay, viability assay, and additional TEM as well as confocal microscopy images are included in the Supporting Information.

All animal work was conducted in animal facilities of the University of Helsinki and approved by the National Animal Experiment Board of Finland.

Supporting Information

Supporting Information is available from the Wiley Online Library or from the author.

Acknowledgements

This work was supported by the Academy of Finland (Grant Nos. 263504, 267497, 273645, 286845, and 297580), Biocentrum Helsinki, University of Helsinki Research Funds, European Research Council (Grant No. 310892), Emil Aaltonen Foundation, Sigrid Juselius Foundation, Instrumentarium Science Foundation, Magnus Ehrnrooth Foundation, and Jane and Aatos Erkko Foundation. The work was carried out under the Academy of Finland's Centres of Excellence Programme (2014-2019) and made use of the Aalto Nanomicroscopy Centre (Aalto NMC) premises.

Conflict of Interest

The authors declare no conflict of interest.

Keywords

dendrons, DNA binding, DNA origami, nanobiomedicine, protein–polymer conjugates

Received: June 1, 2017
Revised: June 15, 2017
Published online: July 24, 2017

[1] M. R. Jones, N. C. Seeman, C. A. Mirkin, *Science* **2015**, *347*, 1260901.
[2] V. Linko, H. Dietz, *Curr. Opin. Biotechnol.* **2013**, *24*, 555.
[3] P. W. K. Rothemund, *Nature* **2006**, *440*, 297.
[4] F. Zhang, J. Nangreave, Y. Liu, H. Yan, *J. Am. Chem. Soc.* **2014**, *136*, 11198.
[5] E. S. Andersen, M. Dong, M. M. Nielsen, K. Jahn, R. Subramani, W. Mamdouh, M. M. Golas, B. Sander, H. Stark, C. L. P. Oliveira, J. S. Pedersen, V. Birkedal, F. Besenbacher, K. V. Gothelf, J. Kjems, *Nature* **2009**, *459*, 73.
[6] S. M. Douglas, H. Dietz, T. Liedl, B. Högberg, F. Graf, W. M. Shih, *Nature* **2009**, *459*, 414.
[7] H. Dietz, S. M. Douglas, W. M. Shih, *Science* **2009**, *325*, 725.
[8] D. Han, S. Pal, J. Nangreave, Z. Deng, Y. Liu, H. Yan, *Science* **2011**, *332*, 342.
[9] Y. Ke, L. L. Ong, W. M. Shih, P. Yin, *Science* **2012**, *338*, 1177.
[10] D. Han, S. Pal, Y. Yang, S. Jiang, J. Nangreave, Y. Liu, H. Yan, *Science* **2013**, *339*, 1412.
[11] E. Benson, A. Mohammed, J. Gardell, S. Masich, E. Czeizler, P. Orponen, B. Högberg, *Nature* **2015**, *523*, 441.
[12] R. Veneziano, S. Ratanalert, K. Zhang, F. Zhang, H. Yan, W. Chiu, M. Bathe, *Science* **2016**, *352*, 1534.
[13] C. E. Castro, F. Kilchherr, D.-N. Kim, E. L. Shiao, T. Wauer, P. Wortmann, M. Bathe, H. Dietz, *Nat. Methods* **2011**, *8*, 221.
[14] V. Linko, M. A. Kostiainen, *Nat. Biotechnol.* **2016**, *34*, 826.
[15] M. Langecker, V. Arnaut, T. G. Martin, J. List, S. Renner, M. Mayer, H. Dietz, F. C. Simmel, *Science* **2012**, *338*, 932.
[16] A. Kuzyk, R. Schreiber, Z. Fan, G. Pardatscher, E.-M. Roller, A. Högele, F. C. Simmel, A. O. Govorov, T. Liedl, *Nature* **2012**, *483*, 311.
[17] A. Gopinath, E. Miyazono, A. Faraon, P. W. K. Rothemund, *Nature* **2016**, *535*, 401.
[18] J. J. Funke, H. Dietz, *Nat. Nanotechnol.* **2016**, *11*, 47.
[19] D. N. Selmi, R. J. Adamson, H. Attrill, A. D. Goddard, R. J. C. Gilbert, A. Watts, A. J. Turberfield, *Nano Lett.* **2011**, *11*, 657.

[20] S. Ramakrishnan, S. Subramaniam, A. F. Stewart, G. Grundmeier, A. Keller, *ACS Appl. Mater. Interfaces* **2016**, *8*, 31239.
[21] V. Linko, S. Nummelin, L. Aarnos, K. Tapio, J. J. Toppari, M. A. Kostiainen, *Nanomaterials* **2016**, *6*, 139.
[22] J. B. Knudsen, L. Liu, A. L. B. Kodal, M. Madsen, Q. Li, J. Song, J. B. Woehrstein, S. F. J. Wickham, M. T. Strauss, F. Schueder, J. Vinther, A. Krissanaprasit, D. Gudnason, A. A. A. Smith, R. Ogaki, A. N. Zelikin, F. Besenbacher, V. Birkedal, P. Yin, W. M. Shih, R. Jungmann, M. Dong, K. V. Gothelf, *Nat. Nanotechnol.* **2015**, *10*, 892.
[23] H. T. Maune, S.-p. Han, R. D. Barish, M. Bockrath, W. A. Goddard III, P. W. K. Rothemund, E. Winfree, *Nat. Nanotechnol.* **2010**, *5*, 61.
[24] S. Helmi, C. Ziegler, D. J. Kauert, R. Seidel, *Nano Lett.* **2014**, *14*, 6693.
[25] W. Sun, E. Boulais, Y. Hakobyan, W. L. Wang, A. Guan, M. Bathe, P. Yin, *Science* **2014**, *346*, 1258361.
[26] B. Shen, V. Linko, K. Tapio, M. A. Kostiainen, J. J. Toppari, *Nanoscale* **2015**, *7*, 11267.
[27] J. Li, C. Fan, H. Pei, J. Shi, Q. Huang, *Adv. Mater.* **2013**, *25*, 4386.
[28] S. Surana, A. R. Shenoy, Y. Krishnan, *Nat. Nanotechnol.* **2015**, *10*, 741.
[29] Y.-J. Chen, B. Groves, R. A. Muscat, G. Seelig, *Nat. Nanotechnol.* **2015**, *10*, 748.
[30] V. Linko, A. Ora, M. A. Kostiainen, *Trends Biotechnol.* **2015**, *33*, 586.
[31] S. M. Douglas, I. Bachelet, G. M. Church, *Science* **2012**, *335*, 861.
[32] Q. Jiang, C. Song, J. Nangreave, X. Liu, L. Lin, D. Qiu, Z.-G. Wang, G. Zou, X. Liang, H. Yan, B. Ding, *J. Am. Chem. Soc.* **2012**, *134*, 13396.
[33] Y.-X. Zhao, A. Shaw, X. Zeng, E. Benson, A. M. Nyström, B. Högberg, *ACS Nano* **2012**, *6*, 8684.
[34] Q. Zhang, Q. Jiang, N. Li, L. Dai, Q. Liu, L. Song, J. Wang, Y. Li, J. Tian, B. Ding, Y. Du, *ACS Nano* **2014**, *8*, 6633.
[35] P. D. Halley, C. R. Lucas, E. M. McWilliams, M. J. Webber, R. A. Patton, C. Kural, D. M. Lucas, J. C. Byrd, C. E. Castro, *Small* **2016**, *12*, 308.
[36] M. Fu, L. Dai, Q. Jiang, Y. Tang, X. Zhang, B. Ding, J. Li, *Chem. Commun.* **2016**, *52*, 9240.
[37] H. Lee, A. K. R. Lytton-Jean, Y. Chen, K. T. Love, A. I. Park, E. D. Karagiannis, A. Sehgal, W. Querbes, C. S. Zurenko, M. Jayaraman, C. G. Peng, K. Charisse, A. Borodovsky, M. Manoharan, J. S. Donahoe, J. Truelove, M. Nahrendorf, R. Langer, D. G. Anderson, *Nat. Nanotechnol.* **2012**, *7*, 389.
[38] V. J. Schüller, S. Heidegger, N. Sandholzer, P. C. Nickels, N. A. Suhartha, S. Endres, C. Bourquin, T. Liedl, *ACS Nano* **2011**, *5*, 9696.
[39] A. Ora, E. Järvihaavisto, H. Zhang, H. Auvinen, H. A. Santos, M. A. Kostiainen, V. Linko, *Chem. Commun.* **2016**, *52*, 14161.
[40] A. H. Okholm, J. S. Nielsen, M. Vinther, R. S. Sørensen, D. Schaffert, J. Kjems, *Methods* **2014**, *67*, 193.
[41] J. Hahn, S. F. Wickham, W. M. Shih, S. D. Perrault, *ACS Nano* **2014**, *8*, 8765.
[42] J. Mikkilä, A.-P. Eskelinen, E. H. Niemelä, V. Linko, M. J. Frilander, P. Törmä, M. A. Kostiainen, *Nano Lett.* **2014**, *14*, 2196.
[43] S. D. Perrault, W. M. Shih, *ACS Nano* **2014**, *8*, 5132.
[44] A. Chopra, S. Krishnan, F. C. Simmel, *Nano Lett.* **2016**, *16*, 6683.
[45] J. Brglez, P. Nikolov, A. Angelin, C. M. Niemeyer, *Chem. Eur. J.* **2015**, *21*, 9440.
[46] D. H. Schaffert, A. H. Okholm, R. S. Sørensen, J. S. Nielsen, T. Tørring, C. B. Rosen, A. L. B. Kodal, M. R. Mortensen, K. V. Gothelf, J. Kjems, *Small* **2016**, *12*, 2634.
[47] J. K. Kiviaho, V. Linko, A. Ora, T. Tiainen, E. Järvihaavisto, J. Mikkilä, H. Tenhu, Nonappa, M. A. Kostiainen, *Nanoscale* **2016**, *8*, 11674.
[48] N. P. Agarwal, M. Matthies, F. N. Gür, K. Osada, T. L. Schmidt, *Angew. Chem., Int. Ed.* **2017**, *56*, 5460; *Angew. Chem.* **2017**, *129*, 5552.
[49] N. Ponnuswamy, M. M. C. Bastings, B. Nathwani, J. H. Ryu, L. Y. T. Chou, M. Vinther, W. A. Li, F. M. Anastassacos, D. J. Mooney, W. M. Shih, *Nat. Commun.* **2017**, *8*, 15654.
[50] S. M. Grayson, J. M. J. Fréchet, *Chem. Rev.* **2001**, *101*, 3819.
[51] D. A. Tomalia, J. B. Christensen, U. Boas, *Dendrimers, Dendrons and Dendritic Polymers*, Cambridge University Press, New York **2012**.
[52] A. W. Bosman, H. M. Janssen, E. W. Meijer, *Chem. Rev.* **1999**, *99*, 1665.
[53] L. Röglin, E. H. M. Lempens, E. W. Meijer, *Angew. Chem., Int. Ed.* **2011**, *50*, 102; *Angew. Chem.* **2011**, *123*, 106.
[54] B. M. Rosen, C. J. Wilson, D. A. Wilson, M. Peterca, M. R. Imam, V. Percec, *Chem. Rev.* **2009**, *109*, 6275.
[55] E. M. Pelegri-O'Day, E.-W. Lin, H. D. Maynard, *J. Am. Chem. Soc.* **2014**, *136*, 14323.
[56] I. Cobo, M. Li, B. S. Sumerlin, S. Perrier, *Nat. Mater.* **2015**, *14*, 143.
[57] X. Huang, M. Li, D. C. Green, D. S. Williams, A. J. Patil, S. Mann, *Nat. Commun.* **2013**, *4*, 2239.
[58] J. M. Hoffman, M. Ebara, J. J. Lai, A. S. Hoffman, A. Folch, P. S. Stayton, *Lab Chip* **2010**, *10*, 3130.
[59] A. Lacroix, T. G. W. Edwardson, M. A. Hancock, M. D. Dore, H. F. Sleiman, *J. Am. Chem. Soc.* **2017**, *139*, 7355.
[60] A. S. Pitek, S. A. Jameson, F. A. Veliz, S. Shukla, N. F. Steinmetz, *Biomaterials* **2016**, *89*, 89.
[61] V. Linko, B. Shen, K. Tapio, J. J. Toppari, M. A. Kostiainen, S. Tuukkanen, *Sci. Rep.* **2015**, *5*, 15634.
[62] E. Stahl, T. G. Martin, F. Praetorius, H. Dietz, *Angew. Chem., Int. Ed.* **2014**, *53*, 12735; *Angew. Chem.* **2014**, *126*, 12949.
[63] M. A. Kostiainen, G. R. Szilvay, D. K. Smith, M. B. Linder, O. Ikkala, *Angew. Chem., Int. Ed.* **2006**, *45*, 3538; *Angew. Chem.* **2006**,*118*, 3618.
[64] M. A. Kostiainen, G. R. Szilvay, J. Lehtinen, D. K. Smith, M. B. Linder, A. Urtti, O. Ikkala, *ACS Nano* **2007**, *1*, 103.
[65] H. Wagner, S. Bauer, *J. Exp. Med.* **2006**, *2*, 265.

